Journal Homepage: http://ijcpe.uobaghdad.edu.iq
Iraqi Journal of Chemical and Petroleum Engineering
Vol. 27 No. 2 (June 2026) 155 – 171
EISSN: 2618-0707, PISSN: 1997-4884

# Studying the effect of different parameters on the oxidation desulfurization of diesel fuel using $Fe_2O_3$-NiO/$SiO_2$ bimetallic catalyst: Experimental and kinetic models

**Mohammed K. Salih [a], Ghassan H. AbdulRazzaq [a], Jasim I. Humadi [a, *]**

*a Department of Petroleum and Gas Refining Engineering, College of Petroleum Processes Engineering, Tikrit University, Tikrit 34001, Iraq*

## Abstract

Given the environmental and health risks posed by sulfur pollutants, their removal and the production of lower sulfur hydrocarbon fuels are essential. Therefore, oxidative desulfurization (ODS) technology has become crucial as it operates efficiently under moderate conditions. This study focused on the synthesis of a ($Fe_2O_3$ + NiO)/$SiO_2$ catalyst via incipient wetness impregnation, followed by drying at 120°C and calcination at 600°C. Several tests were performed on the catalyst before its application: BET, TGA, and SEM-EDX. The BET results showed a decrease in surface area from 166.47 to 149.57 $m^2\ g^{-1}$ after metal loading, confirming the fixation of iron and nickel oxides on the silica support. XRD and FTIR analyses confirmed the formation of the metal oxide phases $Fe_2O_3$ and NiO, while preserving the amorphous nature of the silica. The prepared catalyst was tested in ultrasonic oxidative desulfurization of real diesel fuel containing up to 2018.14 ppm using hydrogen peroxide as the oxidizing agent. Various conditions were investigated, including the effect of temperature (25–75°C), reaction time (30–60 minutes), and ultrasonic intensity (80–100%). This was followed by ethanol extraction at a 1:1 diesel-to-solvent ratio. A sulfur removal efficiency of 90% was achieved. The study showed that the reaction followed a pseudo-first-order model with reaction rate constants of 0.0172, 0.0252, and 0.0400 $min^{-1}$ at 25, 50, and 75°C, respectively, with $R^2$ =0.98. The activation energy of the reaction was also calculated and found to be 14.50 kJ $mol^{-1}$, indicating the suitability of the kinetics and the efficiency of the catalytic activity under the influence of ultrasonication.

*Keywords: oxidative desulfurization (ODS); diesel fuel; silica supports; ultrasonic reactor; Kinetic parameters.*

*Received on 27/05/2026, Received in Revised Form on 22/06/2026, Accepted on 27/06/2026, Published on 30/06/2026*

*https://doi.org/10.31699/IJCPE.2026.2.12*

## 1- Introduction

Many countries are striving to achieve ultra-low sulfur levels in fuel oils and their petrochemical products as a result of stricter regulations on sulfur-containing fuel oils [1], because of Sulfur oxides (SOx), which are generated from the combustion of sulfur compounds in various fuels, are a major source of acid rain, air pollution, catalyst failure, and metal corrosion, in addition to their negative effects on human health [2-5]. Hydrodesulfurization (HDS) is the traditional industrial technique used in oil refineries to remove sulfur compounds from petroleum products. However, this process is undesirable because it requires high hydrogen temperatures and pressures, consumes a significant amount of energy, and has limited efficiency against resistant aromatic sulfur compounds such as dibenzothiophene and its derivatives [1, 3, 5]. Therefore, oxidative desulfurization (ODS) has emerged as a promising alternative due to its ability to operate under moderate conditions and achieve deep sulfur removal, particularly of aromatic sulfur and its derivatives, with lower operational requirements[1, 6, 7]. Oxidative desulfurization (ODS) is one of the alternative technologies that has gained widespread attention in recent decades. Its operating principle is based on converting the sulfur compounds present in the fuel into more polar compounds by oxidizing them and converting them into Sulfoxides and sulfones using an oxidizer of hydrogen peroxide. Then, the oxidized compounds are efficiently removed through a solvent extraction process due to their high polarity compared to the original sulfur compounds [7-9].

The efficiency of the ODS process depends greatly on the characteristics of the catalyst and the oxidizing agent, the reactor design, and the efficiency of mass transfer between the different phases [6, 10]. Silica's high surface area, controllable porosity, and excellent thermal stability have made silica-based catalysts highly attractive, in addition to their ability to effectively disperse active metal species [11-13]. Transition metal oxides such as $Fe_2O_3$ and NiO have also demonstrated good catalytic activity in oxidation reactions due to their ability to promote the formation of active oxygen species and catalyze the oxidation of sulfur compounds [8, 14, 15].In recent years, ultrasonic-assisted oxidative desulfurization has emerged

*Corresponding Author: Email: jasim_alhashimi_ppe@tu.edu.iq

as an effective process intensification technique. Ultrasound induces the formation of cavitation bubbles that collapse violently, generating localized areas of high temperature and pressure. This leads to improved mixing and catalyst dispersion, as well as increased mass transfer between the reacting phases[16-18]. Several previous studies have indicated that using ultrasound significantly improves desulfurization efficiency and reduces reaction time compared to conventional mechanical mixing processes [16, 18]. Previous studies have demonstrated the effectiveness of silica-supported catalysts in oxidative desulfurization applications.

Yan et al. achieved high desulfurization efficiency using silica-supported phosphotungstic acid on $SiO_2$ [17], and Banisharif et al. showed excellent efficiency using silica-stabilized vanadium-substituted polyoxometals [18], and Sundararaman and others using a $MoO_3/SiO_2$ catalyst [19], and Liu and others using the $C_{16}PW/SiO_2$ catalyst [20], and Ghubayra also studied the oxidation reaction using the 15% HPA-1/$SiO_2$ catalyst [21]. In a more recent study, Zahran et al. reported improved diesel desulfurization using ultrasonic-supported catalytic oxidation based on mixed metal oxide complexes followed by solvent extraction [15]. Recent reviews have also highlighted the growing importance of ultrasonic-assisted oxidative desulfurization techniques for producing low-sulfur fuels in an environmentally friendly manner [18, 24]. Despite these advancements, studies on the use of silica-supported $Fe_2O_3$–NiO bimetallic catalysts in ultrasonic-assisted oxidative desulfurization of real diesel fuel remain limited. Furthermore, the combined effect of ultrasonic intensity, temperature, and reaction time on desulfurization efficiency and reaction kinetics has not been adequately investigated. Therefore, this research aims to prepare and characterize a structured ($Fe_2O_3$ + NiO)/$SiO_2$ bimetallic catalyst and evaluate its performance in ultrasonic-assisted oxidative desulfurization of real diesel fuel using hydrogen peroxide as the oxidizing agent. The effects of temperature, reaction time, and ultrasonic intensity on desulfurization efficiency were also investigated. Additionally, kinetic studies and activation energy analysis were conducted to understand the reaction mechanism and evaluate the catalytic performance of the developed catalyst.

## 2- Experimental work

### 2.1. Materials and fuel

In this work, real diesel fuel with a total sulfur content of 2018.14 was used. It was obtained from the North Refineries Company, Baiji Refinery, Salah al-Din Governorate, Iraq. The diesel fuel properties are detailed in Table 1.

**Table 1.** Physical properties of diesel

| Physical property | Diesel |
|---|---|
| Sp.gr@15.6 | 0.8217 |
| Flash point | 62 |
| Total sulphur (ppm) | 2018.14 |
| API gravity | 40.7 |
| Viscosity (sct) @ 40 ℃ | 3.15 |
| Colour | 0.9 |
| **Distillation** | |
| I.B.P ℃ | 175 |
| 5% | 183 |
| 10% | 190 |
| 50% | 252 |
| 90% | 320 |
| 95% | 338 |
| EP% | 354 |

The materials used in preparing the catalyst were silica imported from Shanghai Macklin Biochemical/China, ferric nitrate hydrate (Fe $(NO_3)_3.9H_2O$) with 98% purity, and nickel(II) nitrate hexahydrate (Ni $(NO_3)_2.6H_2O$), both with 99% purity and imported from Central Drug House (CDH). Additionally, utilized were ethanol ($C_2H_5OH$) with 25% purity from RCI LABSCAN LIMITED, hydrogen peroxide ($H_2O_2$) with 35% purity from PanReac AppliChem, and deionized water. In this study, hydrogen peroxide was used based on its key advantage: its decomposition products yield water, eliminating the complex need to dispose of toxic substances produced by other oxidants. Furthermore, it has a high oxygen content relative to its molecular size [9, 25]. As for ethanol, it was chosen because of its availability and safety, being a commercially available polar solvent, low cost, and less toxic than traditional toxic solvents such as acetonitrile or DMF [6, 24].

### 2.2. Preparation of catalyst ($Fe_2O_3$ – NiO / $SiO_2$)

The catalyst was prepared using the Incipient Wetness Impregnation method by dissolving 3.8 g of ferric nitrate hydrate (Fe $(NO_3)_3.9H_2O$) and 2.6 g of nickel nitrate hexahydrate (Ni $(NO_3)_2.6H_2O$) in 50 mL of deionized water. The prepared solution was then stirred for 1 hour using a magnetic stirrer until the salts were completely dissolved. Next, 10 g of commercial silica was gradually added, and the resultant slurry was stirred again using a magnetic stirrer. Finally, the obtained suspension was ultrasonically stirred for 2 hours to ensure complete dissolution. The wet composite was then dried overnight in a drying oven at 120°C. After drying, the sample was

calcined in a tubular furnace at a temperature gradient: 200°C for 1 hour, 400°C for 1 hour, and finally 600°C for 4 hours. The calcined solid was then ground to produce the ready-made catalyst, as illustrated in Fig. 1.


**Fig. 1.** Preparation of catalyst ($Fe_2O_3$ – NiO / $SiO_2$) by the impregnation method

2.3. Catalyst characterization

Several tests were conducted to verify the prepared catalyst ($Fe_2O_3$ – NiO/$SiO_2$), which were performed at the Photon Center, its accredited center. These tests included: Crystalline phases and structural parameters were evaluated by X-ray diffraction (XRD) using a Philips PW1730 X-ray generator coupled with a PW1050 goniometer (Philips, The Netherlands), powered by a Cu Kα copper radiation source. Specific surface area, pore size, and diameter distribution were determined by nitrogen ($N_2$) adsorption and desorption isotherm at 77 K using a BELSORP-mini II analyzer equipped with a Belprep II degassing unit (Microtrack BET, Japan), after pre-treatment of the samples at 120 °C for 2 hours. Surface morphology and elemental composition were examined using field-emission scanning electron microscopy (FE-SEM, TESCAN MIRA3 model, Czech Republic) coupled with an energy-dispersive X-ray spectrometer (EDX, Oxford Instruments AZtec System, UK). The thermal stability and weight loss behavior of the catalyst sample were also monitored by thermogravimetric analysis (TGA) using a Q50 thermogravimetric analyzer (TA Instruments, USA) under controlled atmospheres. Finally, the surface functional groups and chemical bonding states were determined by Fourier transform infrared spectroscopy (FTIR) in the 4000–400 $cm^{-1}$ range using a JASCO FT/IR-4600 spectrometer (JASCO, Japan).

2.4. Experimental Procedure

2.4.1. Oxidative- extraction (OEDS) desulfurization process

The desulfurization of diesel fuel was carried out using an oxidative desulfurization technique enhanced by extraction. A sonic wave reactor (manufactured by a Chinese company) was used for this purpose, as shown in Fig. 2. The oxidation process was carried out using a prepared catalyst (Fe-Ni/SiO2) in the presence of the oxidizing agent, hydrogen peroxide ($H_2O_2$). The fuel used contained 2018.14 ppm of sulfur compounds. 0.5 g of the prepared catalyst (Fe-Ni/ $SiO_2$) was added to every 20 mL of diesel fuel, and 2 mL of the oxidizing agent ($H_2O_2$) was added to each experiment under atmospheric pressure. The process was carried out under moderate conditions at different temperatures (25, 50, and 75 °C) and reaction times (30, 45, and 60 minutes), and at different ultrasonic amplitude levels (80%, 90%, and 100% of the total power of 650 W) in a 20 kHz ultrasonic reactor. Notably, the ultrasonic irradiation relies on localized microfluidic flow and acoustic cavitation rather than conventional mechanical rotation (rpm).

These high-frequency waves generate rapid dispersion and enhance the transfer of material between the immiscible liquid phases and the solid catalyst. Following the ODS process, a 9 cm filter paper was used to separate the solid catalyst from the liquid phase. The remaining liquid, containing highly polar oxidized sulfoxides and sulfons, was then mixed with ethanol, a readily available, inexpensive, and polar solvent, at a 1:1 volumetric ratio. This ratio ensured complete extraction of the sulfons and sulfates and eliminated any mass transfer constraints, allowing for the evaluation of the performance of the prepared catalyst ($Fe_2O_3$–NiO/$SiO_2$). Solvent recovery can be achieved through efficient and low-energy methods, as ethanol has a relatively low boiling point (around 78°C) and a low latent heat of vaporization compared to other solvents.

This enables its recovery via rapid distillation, reducing operating costs and simplifying the process. Furthermore, research has employed ratios higher than 1:1 [25, 26]. Because sulfoxides and sulfones are polar components,

they dissolve readily in ethanol, unlike diesel fuel, in which they are difficult to remove. Based on the principle of density, diesel is separated from other components, as shown in Fig. 3. The diesel fuel is then drawn from the top to obtain clean diesel. The apparatus used to test the sulfur content is manufactured by XOS in the USA and is called the Sandy. Its operating principle is based on longitudinal X-ray diffraction (MWDXRF), which is considered the best method for determining the sulfur content in hydrocarbon fuels. It measures the total sulfur content according to ASTM D7039 standards. The desulfurization efficiency was calculated using Eq. 1

$$convegen = \left(\frac{C_o - C_{OUT}}{C_o}\right) \times 100\ \% \quad (1)$$

Where $C_0$: initial concentration of sulfur, $C_{OUT}$: final concentration of sulfur.

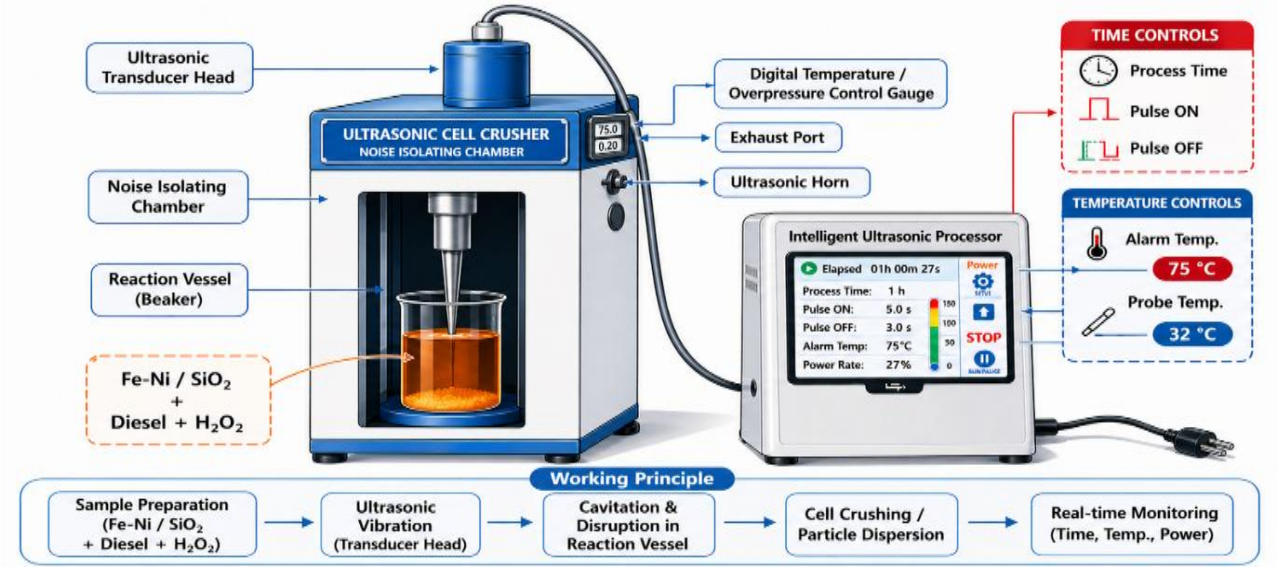


**Fig. 2.** Ultrasonic reactor

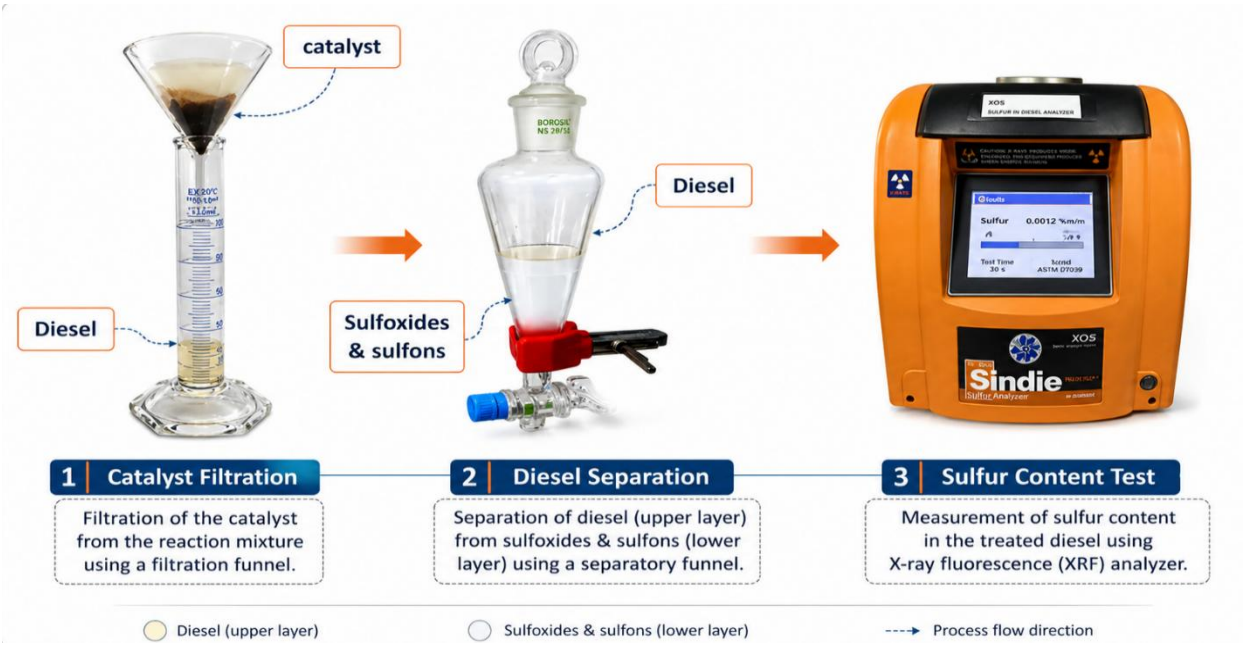


**Fig. 3.** Ethanol extraction process

## 3- Results and discussion

### 3.1. Catalyst characterization

#### 3.1.1. Surface area and pore volume analysis

The study used a BET assay to examine the properties of a silica substrate before and after metal loading, employing a nitrogen adsorption-desorption technique. The isotherm also illustrates this in Fig. 4 a, b. The test was performed at 77 K, with an adsorption cross-sectional area of 0.162 $nm^2$. The analysis showed that the silica before loading possessed good surface area and pore volume. After loading the metals (iron and nickel), the test revealed a decrease in surface area and pore volume. This partial blockage is attributed to the silica pores being

filled with particles of the loaded metal oxides, and the active sites on the silica substrate being covered with these oxides. This change in pore volume and surface area indicates the success of the metal loading process on the substrate, as metal deposition reduces available porosity due to the occupation of internal pores and surface blockage [25]. The slight change in pore diameter after metal loading indicates that the mesoporous silica structure retained its shape, demonstrating that the support retained its structural stability. In addition, the decrease in surface area after loading is due to strong bonding between the loaded metals and the support, where iron and nickel species are bonded to the silica surface and internal pore walls. Table 2 shows the surface area and pore volume before and after metal loading.

**Table 2.** BET, pd, and pv of prepared silica supports and catalysts

| Sample | Surface area ($m^2/g$) | Mean pore diameter (nm) | Total pore volume ($cm^3/g$) |
|---|---|---|---|
| $SiO_2$ | 166.47 | 22.011 | 0.916 |
| ($Fe_2O_3$ + NiO) / $SiO_2$ | 149.57 | 5.5733 | 0.2084 |

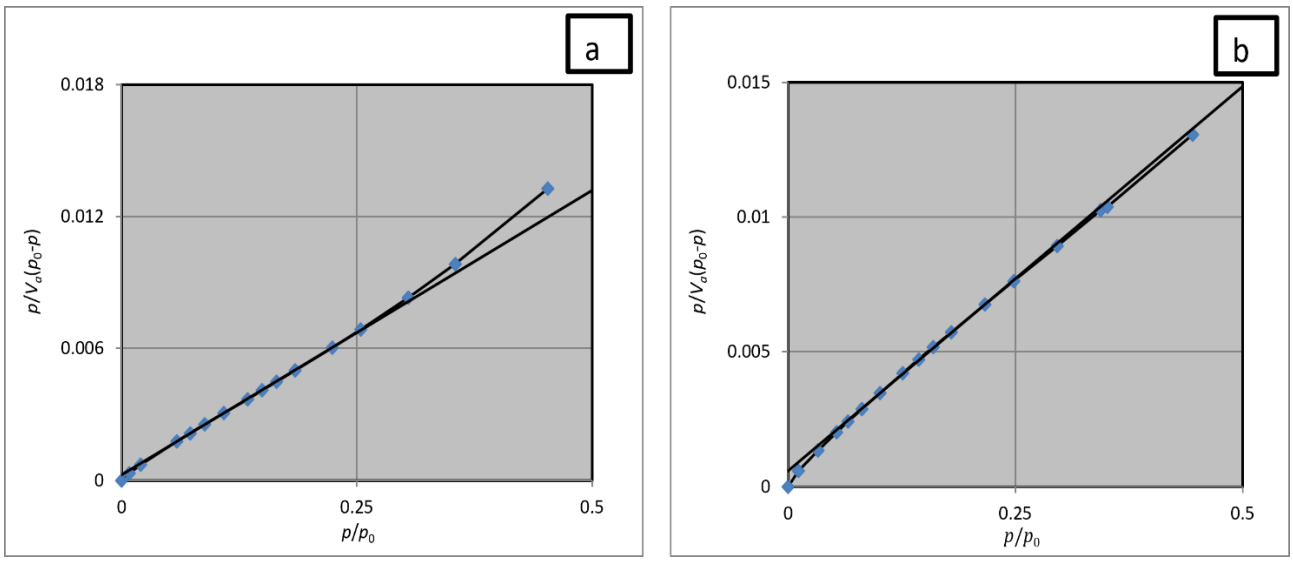


**Fig. 4**. isotherm of BET of (a) $SiO_2$ / (b) $Fe_2O_3$-NiO/$SiO_2$

3.1.2. X-ray diffraction analysis

Fig. 5 shows the X-ray diffraction (XRD) pattern of the silica support before and after metal loading. The scan was performed within the starting position [°2θ]= 9 and the ending position [°2 θ]= 79, with a wavelength λ = (0.15406 nm). Fig. 5 a shows a broad, dispersed halo starting in the 15–30° angular range and centering at 2θ ≈ 22–24°, a range characteristic of amorphous silica ($SiO_2$)[11,26]. The absence of sharp peaks in the sample indicates a lack of crystalline order, confirming that the support is primarily composed of an irregular siloxane lattice. Following the metal loading process (nickel and iron), Fig. 5 b retains the characteristic broad halo of silica centered at 22–24°, indicating that the amorphous silica substrate retained its structure after impregnation. Additional diffraction peaks were also observed at approximately 2θ ≈ 36–37°, 57–58°, 43–44°, and 63–64°.These values correspond to crystalline phases of NiO and $Fe_2O_3$, consistent with previous studies[13,27,28]. Maintaining the structure of the silica support after metal loading and the appearance of NiO and $Fe_2O_3$ peaks indicates that the active oxides have been well distributed on the support surface without affecting its amorphous nature.

3.1.3. Fourier transform infrared (FTIR) analysis

The FTIR spectrum of unloaded amorphous silica Fig. 6 a reveals the characteristic siloxane network structure. A major peak at ~1080–1100 $cm^{-1}$ is attributed to the asymmetric tensile vibration of the Si–O–Si bonds. Peaks at ~800 $cm^{-1}$ are attributed to symmetric tensile vibration, and peaks at ~470 $cm^{-1}$ to curvature. A weak peak at ~950–970 $cm^{-1}$ may be due to silanol groups (Si–OH), However, at around ~140٢.9 $cm^{-1}$, $Si–O^-$ groups may be distinguished, confirming the hydroxyl nature of the silica surface [29-32]. In addition, the peaks at ~3400–3200, 3700 $cm^{-1}$ $cm^{-1}$ may be due to the elongation vibrations of the surface hydroxyl groups (O–H) and the actually absorbed water, and the peaks at ~1600 $cm^1$ are due to the bending vibrations of the water (H–O–H), indicating the hydrophilic nature of the support surface [29-33]. The band at around 2356.5 $cm^{-1}$ is attributed to ambient carbon dioxide absorption, which typically appears in FTIR spectra due to interference from the surrounding air and the infrared pathway [34, 35].

Consequently, this peak is thought to be a result of spectrum interference rather than the chemical makeup of the material. Fig. 6 b shows clear changes after loading iron and nickel, especially in the low region located within the wavelength range at (400–800 $cm^{-1}$), In this range, the peaks of the metal-oxygen bond are found, as

the appearance of new peaks 620.9, 539.9, 470.5, 447.4 is attributed to the metal oxides Fe–O and Ni–O, while maintaining the basic peaks of the support before loading. This confirms the success of the deposition of metal oxides on the silica surface [36, 37]. The slight decrease in the moxibustion bands after loading indicates coverage of these aggregates and confirms the interaction of the support with the metal [38].

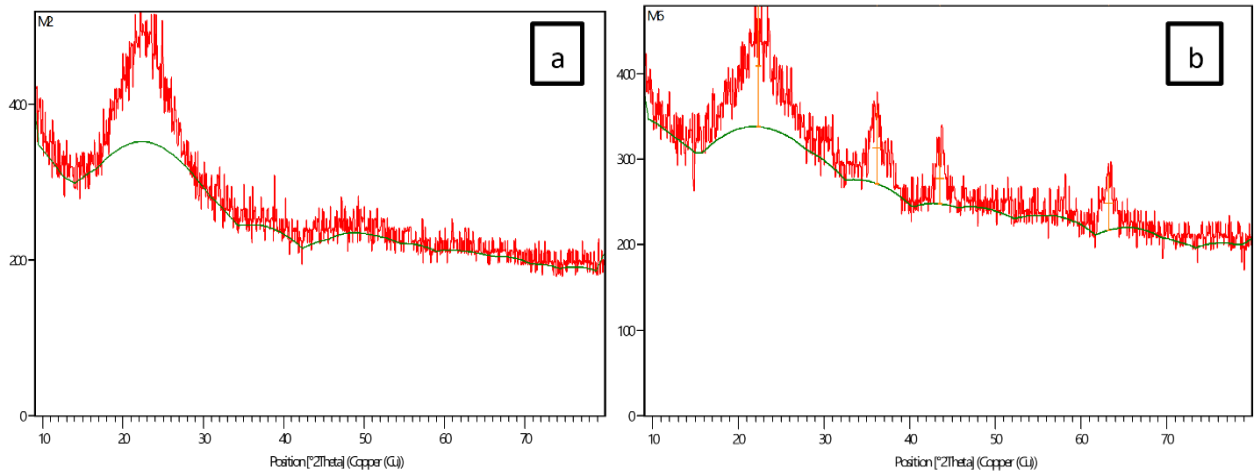


**Fig. 5.** The X-ray diffraction (XRD) pattern of (a) $SiO_2$ / (b) $Fe_2O_3$-NiO/$SiO_2$

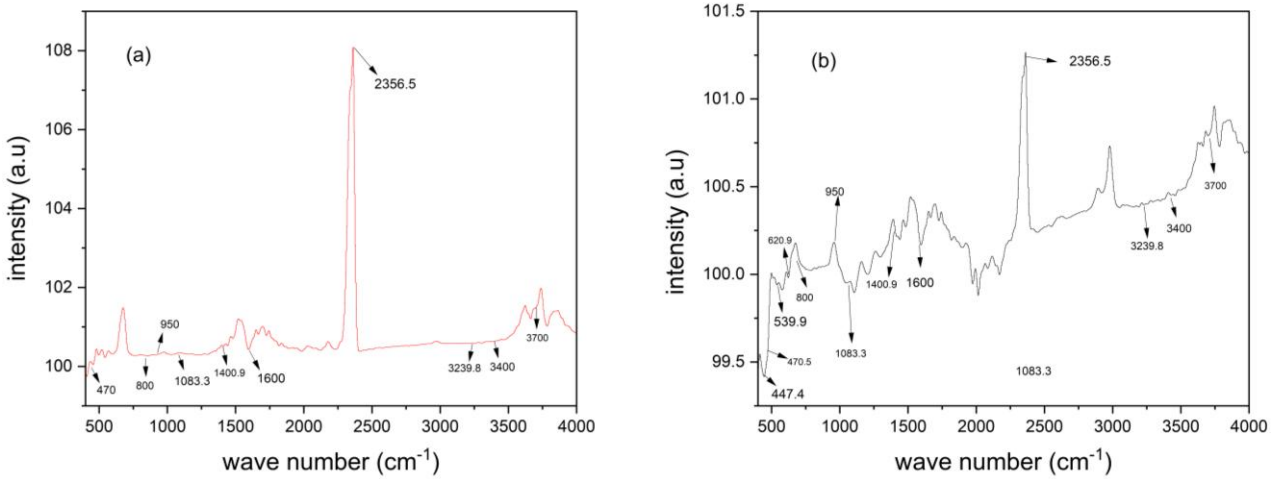


**Fig. 6.** FTIR analysis of (a) $SiO_2$ / (b) $Fe_2O_3$-NiO/$SiO_2$

3.1.4. Thermal Gravimetric Analysis (TGA)

Fig. 7 shows the thermogravimetric analysis (TGA) curves for the silica support and the iron-nickel-loaded silica, revealing a significant difference in thermal behavior. This reflects the change in structure and surface properties after metal loading. The silica support in Fig. 7 a exhibits a total weight loss of approximately 61.55% within the temperature range of 25–600 °C. This demonstrates the high density of hydroxyl groups (Si–OH) and the silica's ability to retain moisture within its porous structure. The weight loss in the first phase (25–200 °C), approximately 28.44%, may indicate the removal of physically adsorbed water weakly bound to the silica surface, and the second phase (200–300 °C), with a weight loss of 7.35%, represents the beginning of silanol condensation and for the third stage (300–600 °C), where a significant loss of up to about 25.75% is observed, it is attributed to the gradual removal of hydroxyl groups (dehydroxylation) and the formation of siloxane bonds (Si–O–Si) [12, 39]. This indicates a structural rearrangement and a gradual increase in the thermal stability of the silica. Fig. 7 b represents the silica support after iron and nickel loading, showing a significant decrease in weight loss of approximately 17.31%, indicating a marked improvement in thermal stability after metal loading compared to the silica support before loading.

The loss decreases to approximately 8.78% at 25–200 °C, indicating a reduction in water absorption due to surface coating and pore occupancy by the metal particles. The loss also decreases at 200–300 °C (approximately 2.99%), reflecting a decrease in the density of the silanol groups due to the strong interaction between the silica surface and the oxides. In the 300–400 °C range, the limited loss (approximately 2.45%)

confirms the inhibition of advanced dehydroxylation processes. Finally, at temperatures above 400 °C, the weight loss is approximately 3.091%, indicating the formation of a more stable structure, where the metal oxides enhance structural bonding and reduce thermal fluctuations.

3.1.5. Scanning Electron Microscope- energy-dispersive X-ray (SEM-EDX)

The scanning electron microscopy (SEM) images shown in Fig. 8 a, b at magnifications of 1 μm and 200 nm, respectively, clearly depict the morphology of silica. As seen in the images before the addition of metals, the silica exhibits an amorphous structure composed of relatively closely packed, quasi-spherical nanoparticles of small size that aggregate into loose clumps with distinct interstitial spaces, reflecting an open, mesoporous nature. The primary particles exhibit a characteristically rough surface, which is associated with high surface energy and the presence of silanol groups, promoting agglomeration without compromising available porosity. Fig. 8 c, d shows the silica support after metal loading (iron and nickel) at the same magnification levels. A significant change in surface structure is observed, exhibiting more agglomeration and greater cohesion compared to the substrate before loading, along with a decrease in interfacial spaces. This may indicate partial pore blockage due to the deposition of iron and nickel within the pore channels and on the surface. Brighter and relatively larger areas are also observed, attributed to the formation of iron and nickel oxide particles dispersed on the silica substrate. At high magnification, the primary silica particles appear partially covered by a metallic layer, leading to increased surface roughness and heterogeneity, which is evidence of a strong interaction between the metal and the support.

The EDX spectra of silica before and after iron and nickel loading show some changes in the substrate due to the introduction of binary metal species. Fig. 9 a shows the silica before iron and nickel addition, where only two distinct peaks are present: one for oxygen at (~0.52 keV) and the other for silicon at (~1.74 keV), confirming the formation of a high-purity, impurity-free $SiO_2$ structure. In Fig. 9 b, after metal addition, additional distinct peaks appear, attributed to iron and nickel. The peaks at approximately 0.7 keV (L line) and 6.4 keV (Kα line) are characteristic of iron, while the nickel peaks appear at approximately 0.85 keV and in the range of 7.5–8.3 keV, consistent with the characteristic emission lines of these elements. The presence of Si, O, Fe, and Ni together confirms the successful loading of binary metal species onto the silica substrate. Furthermore, the absence of any additional unwanted peaks indicates that the loading process did not introduce any unwanted impurities. EDX analysis also reveals the preservation of the silica structure, with the appearance of silicon and oxygen peaks, while the presence of iron and nickel reflects effective surface modification, resulting in the formation of an Fe–Ni/$SiO_2$ catalytic system.

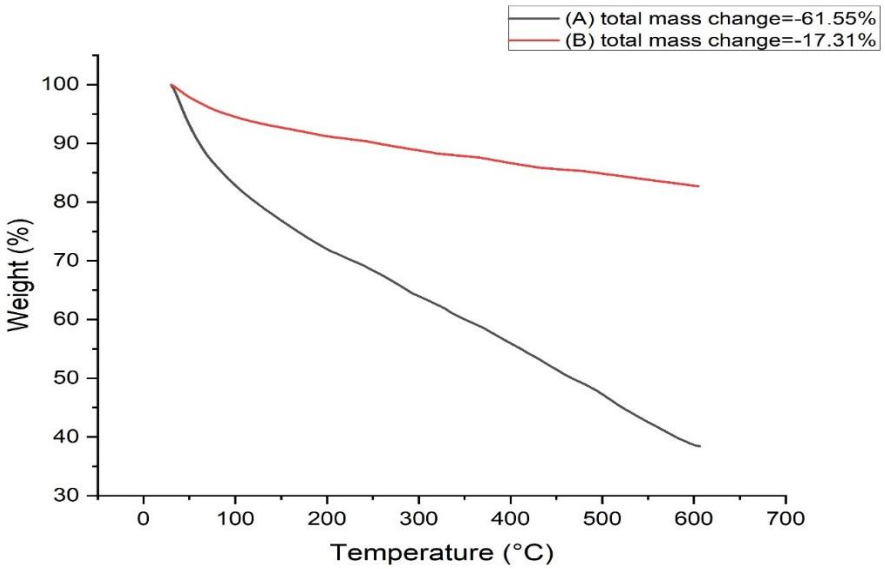


**Fig. 7.** TGA analysis of (a) $SiO_2$ / (b) $Fe_2O_3$-NiO/$SiO_2$

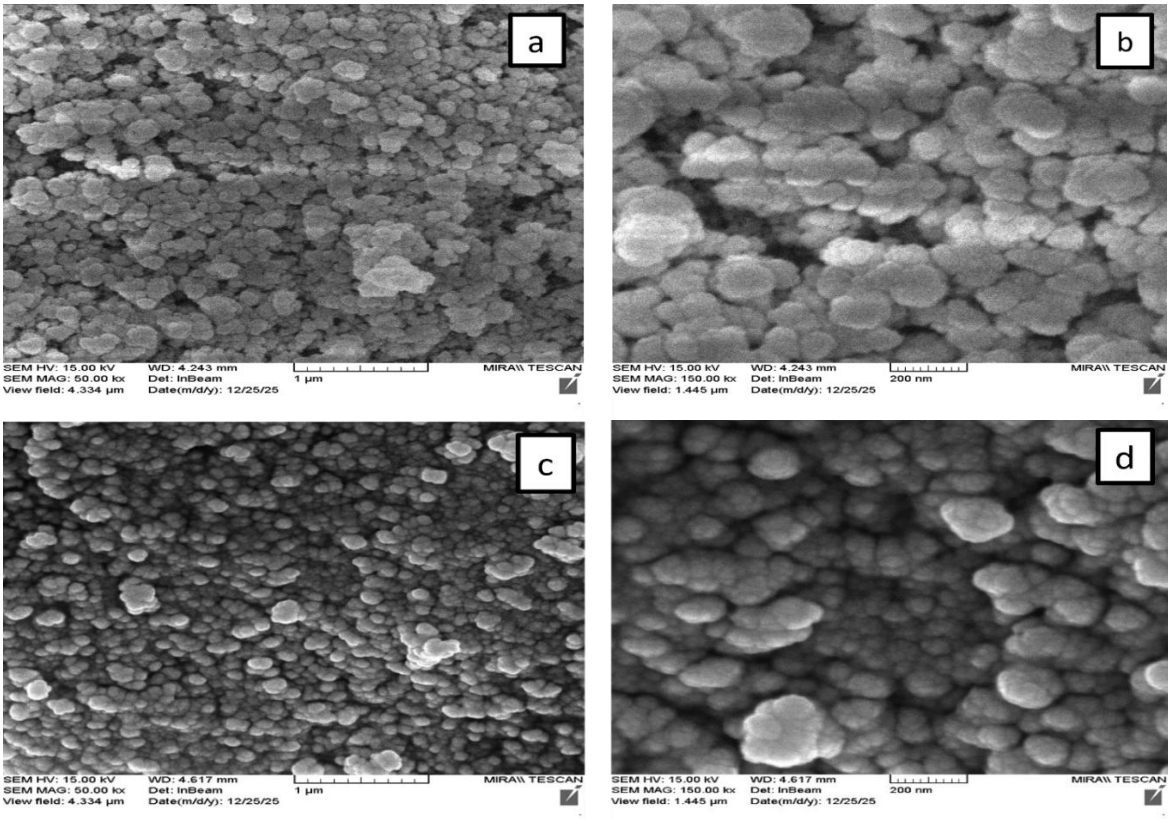


**Fig. 8.** SEM analysis of (a,b) $SiO_2$ / (c,d) $Fe_2O_3$-NiO/$SiO_2$

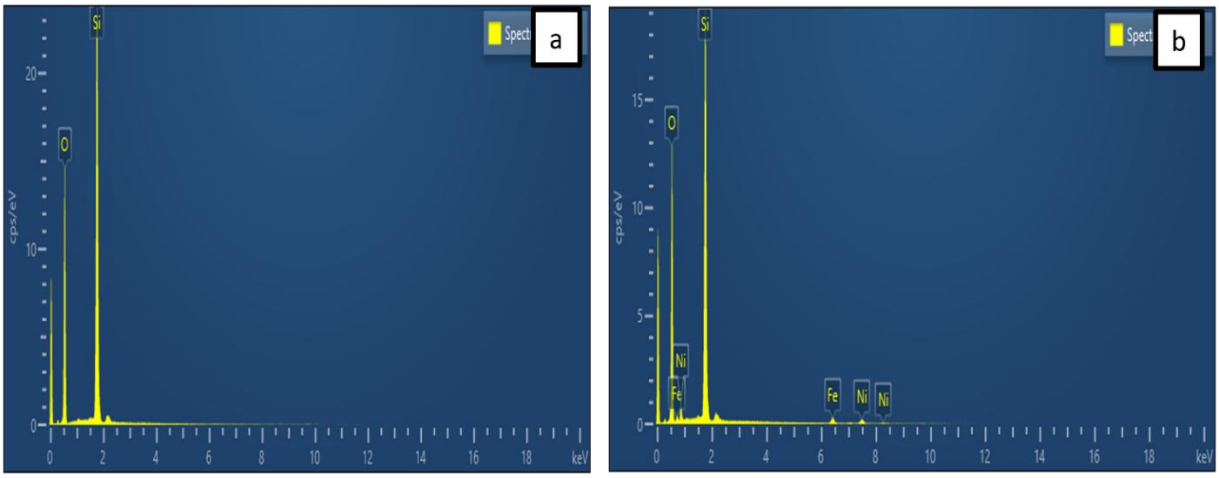


**Fig. 9.** EDX analysis of (a) $SiO_2$ / (b) $Fe_2O_3$-NiO/$SiO_2$

3.2. Oxidative desulfurization performance

3.2.1. Effect of temperature

Temperature is one of the main factors that significantly affects the oxidative desulfurization process. Fig. 10 A-C illustrates how temperature changes affect desulfurization efficiency. Diesel was used with a reaction time of 60 minutes and an ultrasonic mixing efficiency of 80%–100%. Dynamically, raising the reaction temperature from 25°C to 50°C, and finally to 75°C, resulted in a sharp increase in the performance of the sulfur removal rate, with the efficiency reaching a peak of 90% at 75°C with a sound intensity of 100%. where the experimental results clearly showed that the efficiency of the ODS process is highly sensitive to reaction temperature, with the desulfurization efficiency increasing significantly as the temperature rose from 25°C to 75°C.

This increase is primarily attributed to the thermal acceleration of the chemical oxidation steps across the phase boundary. Furthermore, the relationship between diesel viscosity and temperature is inverse; therefore, a significant decrease in viscosity occurs with increasing temperature, promoting the faster migration of sulfur compounds to the catalytically active sites of the ($Fe_2O_3$ + NiO)/$SiO_2$ bimetallic catalyst. As a result, the removal rate increases. Raising the molecules' activation energy results in a significant increase in the number of

molecules engaged in the process, which enhances the removal efficiency since the molecules' activation energy is dependent on the reaction rate constant [40]. The calcination temperature of the generated (Fe- Ni) / $SiO_2$ material may also affect the acid site density, increasing the removal rate [41]. However, excessive ultrasonic temperatures can negatively impact the desulfurization process, as very high temperatures destabilize the catalyst structure, potentially reducing access to active sites [15].

### 3.2.2. Effect of reaction time

As shown in Fig. 11 A, B, C for operating durations of 30, 45, and 60 minutes, with a temperature range of 25-75°C and an ultrasonic efficiency of 80%-100%, increasing the reaction time during ultrasonic mixing enhances ODS desulfurization. For example, under optimal operating conditions of 75°C and 100% ultrasonic power, extending the duration from a short 30 minutes to a medium 45 minutes, and finally to 60 minutes, reduced the total sulfur concentration from its initial heavy charge of 2018.14 ppm to approximately 201.8 ppm (based on a 90% removal efficiency). This increase in reaction time is caused by the increased contact time between the reactants and the catalyst, which accelerates their oxidation in the presence of the oxidizing agent [42, 43]. Furthermore, the longer response time allows for increased mass transfer, which enhances the interaction among the diesel, the catalyst, and the oxidizer, thereby increasing the rate of desulfurization [44-46]. However, increasing the reaction time beyond the permissible limit may negatively affect the ODS process, as the catalyst may become less active due to toxicity, thus reducing the absorption of sulfur compounds and consequently their oxidation, or it may lead to side reactions such as oxidative decomposition or oxidation of hydrocarbon compounds [15]. Therefore, the best removal was obtained at 60 minutes, 75°C, and 100% ultrasonic mixing intensity, as these are considered optimal conditions.

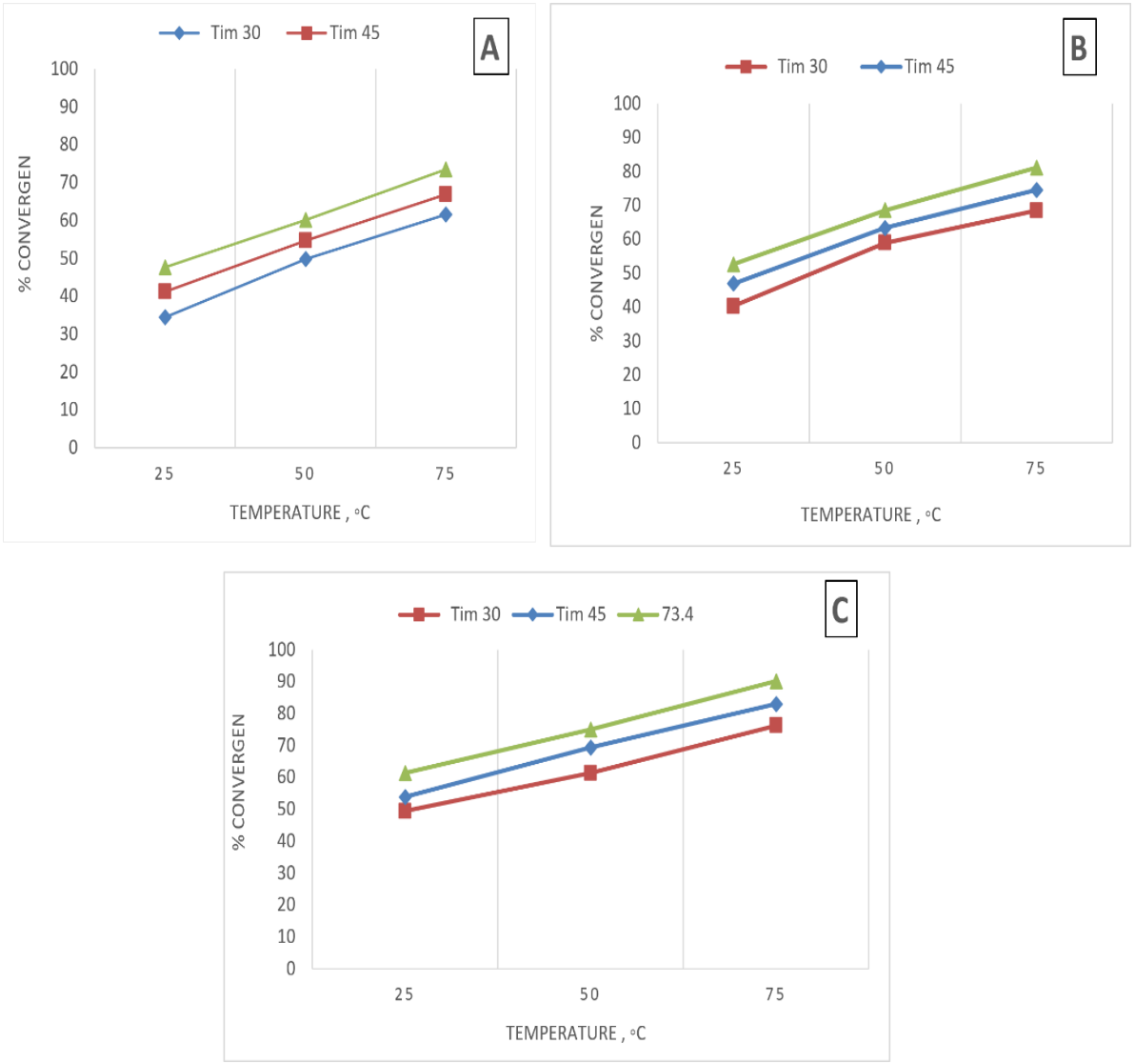


**Fig. 10.** Effect of temperature on ODS at ultrasonic efficiency: (A) 80%, (B) 90%, (C) 100%. The constant variables are: time =60 min, catalyst =0.5 g, diesel=20 ml, and $H_2O_2$ =2 ml

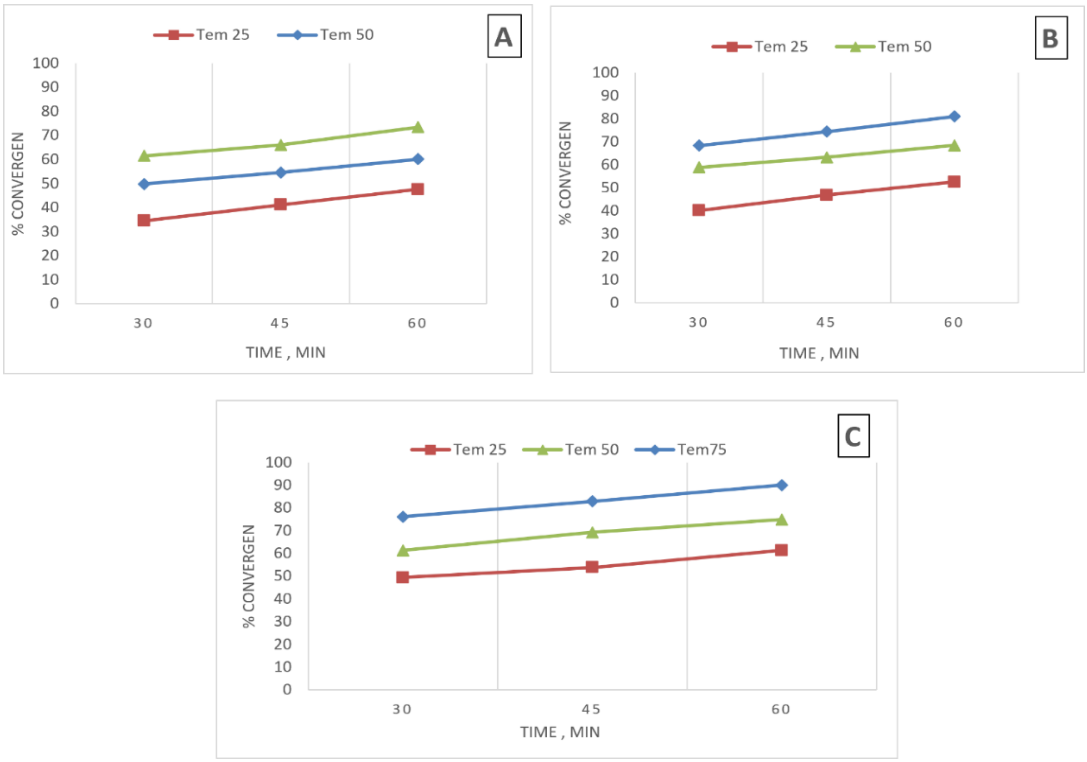


**Fig. 11.** Effect of reaction time on ODS at ultrasonic efficiency: (A) 80%, (B) 90%, (C) 100%. The constant variables are: temperature =75°C, catalyst =0.5 g, diesel=20 ml, and $H_2O_2$ =2 ml

3.2.3. Effect of ultrasonic efficiency

Ultrasonic mixing intensity is a crucial factor in oxidative desulfurization (ODS) and positively impacts the removal efficiency of sulfur compounds. Therefore, this study investigated different mixing efficiencies (80%, 90%, and 100%) for diesel fuel desulfurization, as illustrated in Fig. 12. The study demonstrated that removal efficiency increases with increasing probe efficiency. This is attributed to the increased mass transfer between the two phases (catalyst and diesel), as well as the production of emulsions that enhance the reaction between the reactants [1, 47]. Consequently, the optimal removal efficiency was achieved at 100% mixing efficiency, a temperature of 75°C, and a time of 60 minutes. It should be noted that the primary objective of studying different ultrasonic intensities (80%, 90%, and 100%) was to evaluate their effect on the efficiency of sulfur removal from diesel and to study the reaction performance.

The actual electrical energy consumption at each operating intensity was not directly monitored or measured during the experiments, even though the ultrasonic reactor used in this study had a nominal power of 650 W. Therefore, a precise assessment of the specific energy consumption (kWh) and a detailed economic and technical study of the process were beyond the scope of this study. However, the results clearly showed that increasing the ultrasonic intensity led to an increase in the sulfur removal efficiency from 73.4% to 90% under the same operating conditions. Future studies recommend directly measuring the electrical energy consumption to determine the energy efficiency and economic feasibility of ultrasonic-assisted oxidative sulfur removal processes.

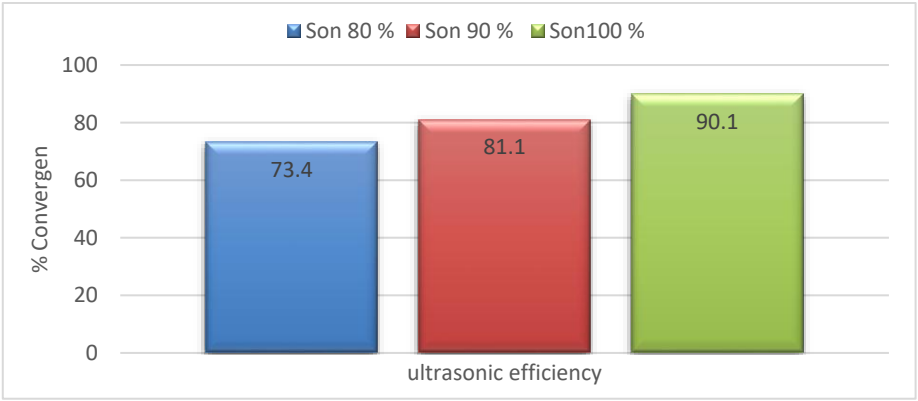


**Fig. 12**. Effect of ultrasonic efficiency on ODS at 60 min and temperature of 75°C. The constant variables are: catalyst =0.5 g, diesel=20 ml, and $H_2O_2$ =2 ml

3.3. Kinetic analysis of oxidative desulfurization

To evaluate the catalytic performance of the prepared catalyst ($Fe_2O_3$ + NiO)/$SiO_2$ and to understand the reaction pathways under the influence of acoustic cavitation, a pseudo-first-order and pseudo-second-order kinetic model was studied using the following equations:
pseudo-first-order:

$$\ln(\frac{C_o}{C_t}) = k_1.t \quad (2)$$

pseudo-second-ord

$$\frac{1}{c_t} - \frac{1}{c_o} = k_2.t \quad (3)$$

Where $C_o$ represents the initial sulfur concentration at (ppm), $C_t$ is the sulfur concentration at time (t) at (ppm), $k_1$ is the rate constant for the pseudo-first-order model ($min^{-1}$) , and $k_2$ $k_1$ is the rate constant for the pseudo-second-order model ($ppm^{-1}. min^{-1}$)

The kinetic study, as shown in Fig. 13 A, B, C considered $\ln(C_o/C_t)$ versus reaction time, and Fig. 14 A, B, C considered ($1/C_t$ - $1/C_o$) versus reaction time. at different temperatures (25, 50, and 75 °C) at 100% acoustic mixing intensity, showed a difference in the correlation coefficients ($R^2$), as shown in Table 3. At temperatures (25 and 50 °C), the second-order expression exhibits a remarkably high linear fit, achieving high $R^2$ values of 0.9933 and 0.9996, respectively. This performance indicates that at low temperatures, the overall ODS rate is mutually limited by the interfacial concentrations of both sulfur compounds and active oxidizing radicals, which is usually governed by significant resistances to phase transition [48].

Conversely, when the temperature is raised to the optimum threshold of 75 °C, a clear kinetic shift is recorded. The pseudo-first-order model exhibits a dominant linear correlation ($R^2$ = 0.9941), consistent with systems operating in excess of the oxidizing agent, where the reaction rate becomes primarily dependent on the concentration of residual sulfur compounds in the reaction medium [49]. In contrast, the conformance of the second-order model drops significantly to 0.9719. This marked shift in $R^2$ trends is physically justified by the decrease in diesel oil viscosity and the simultaneous enhancement of molecular diffusion pathways at elevated temperatures, thereby improving phase-to-phase transport. Furthermore, ultrasonic irradiation induces intense micromixing and microemulsification of the immiscible phases, increasing the interfacial space available for reaction and significantly improving mass transfer rates [48]. At 75°C, the synergistic effect of thermal energy and acoustic cavitation induced by the ultrasound waves further reduces the constraints on mass transfer, ensuring a higher abundance and more homogeneous diffusion of oxidizing species within the reaction medium. As a result, the reaction becomes more subject to the concentration of sulfur compounds rather than to translocation phenomena, making its kinetic behavior closer to a pseudo-first-order model than to a pseudo-second-order model [48, 50].

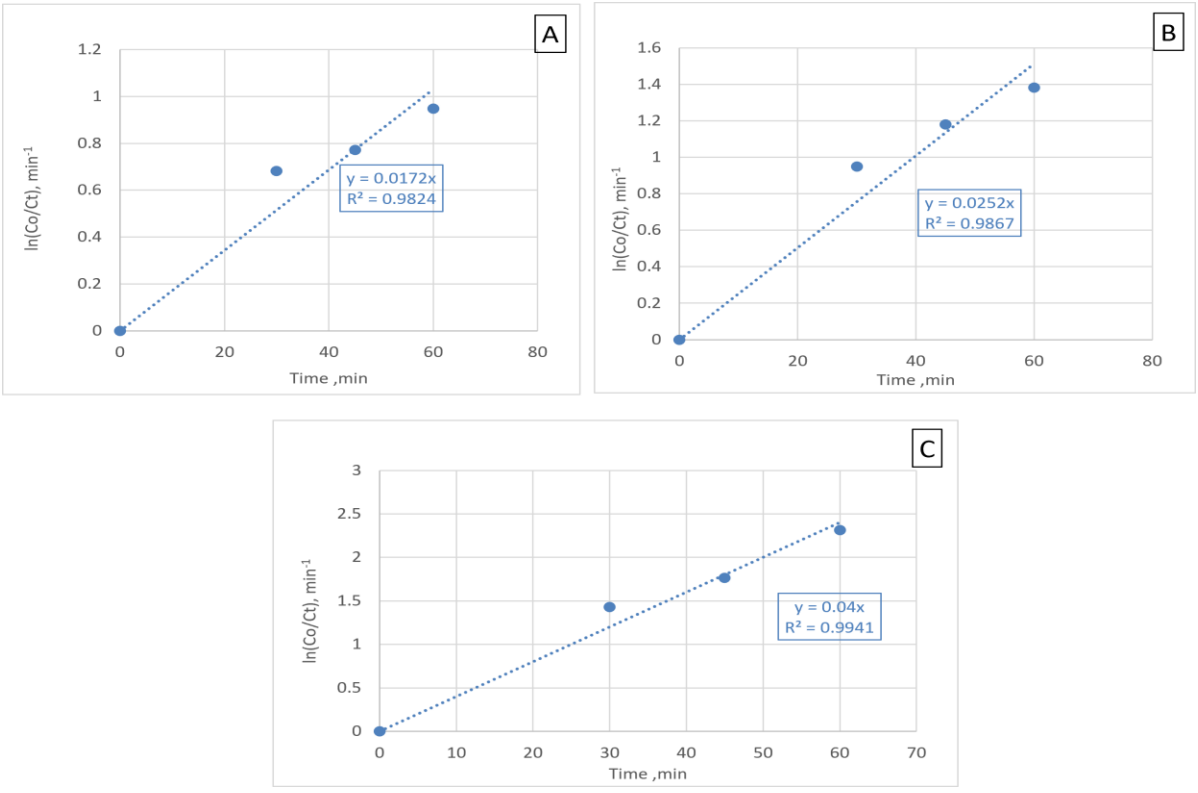


**Fig. 13.** Ln ($C_t$ / $C_O$) versus (t) of sulfur oxidation reactions using the prepared nano-catalyst (A) at 25 °C, (B) at 50 °C, (C) at 75 °C

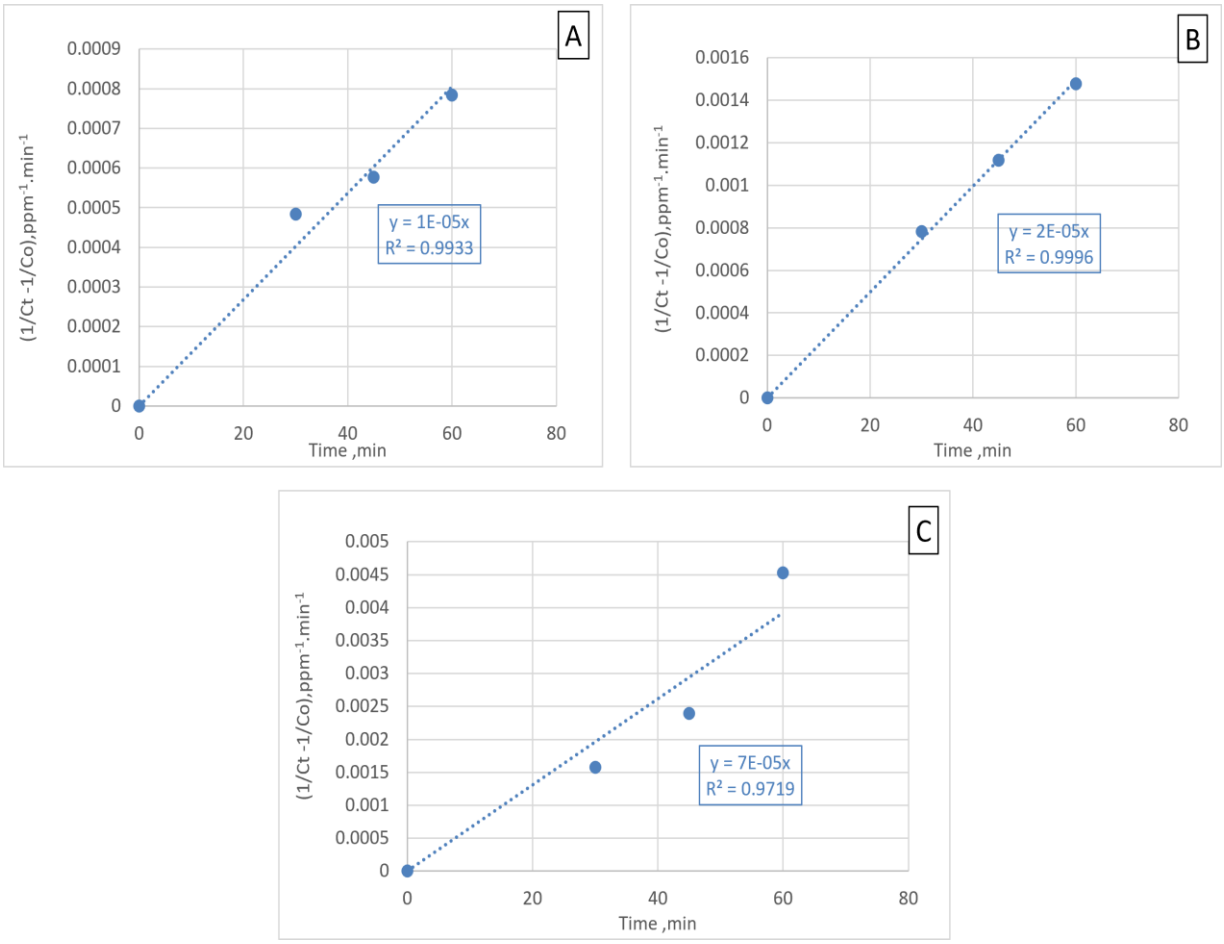


**Fig. 14.** (1/Ct -1/Co), versus (t) of sulfur oxidation reactions using the prepared nano-catalyst (A) at 25 °C, (B) at 50 °C, (C) at 75 °

**Table 3.** Kinetics models result in ODS

| Order of Reaction | K=constant | $R^2$ |
|---|---|---|
| **T= 25 °C** | | |
| The pseudo-first order | 0.0172 ($min^{-1}$) | 0.9824 |
| The pseudo-second-order | $1*10^{-5}$($ppm^{-1}.min^{-1}$) | 0.9933 |
| **T= 50 °C** | | |
| The pseudo-first order | 0.0252 ($min^{-1}$) | 0.9867 |
| The pseudo-second-order | $2*10^{-5}$($ppm^{-1}.min^{-1}$) | 0.9996 |
| **T= 75 °C** | | |
| The pseudo-first order | 0.04 ($min^{-1}$) | 0.9941 |
| The pseudo-second-order | $7*10^{-5}$ ($ppm^{-1}.min^{-1}$) | 0.9719 |

Finding the apparent activation energy of the ODS reaction using ultrasonication based on the Arrhenius equation is as follows:

$$k = k_o e^{-\frac{E_a}{RT}} \quad (6)$$

$$\ln(k) = lnk_o - \frac{E_a}{RT} \quad (7)$$

Where $k_o$: is the Pre-exponential factor, $E_a$: is the apparent activation energy (kJ/mol), T:is the oxidation temperature (K), and R: is the gas constant (kJ/mole. K).

Fig. 15 clearly shows the (-ln k) versus (1/T) plot, indicating a linear trend in these data. The correlation coefficient $R^2$ = 0.99 is shown, and the data plot reveals an activation energy of E=14.50 kJ/mol for desulfurization using an ultrasonic reactor. This low activation energy suggests that the ODS technology and the catalyst are capable of rapidly oxidizing sulfur compounds in diesel with less energy. This is supported by the high removal rate (90%) achieved within 60 minutes. Furthermore, this can be explained by the increased electron density of the sulfur compounds, resulting in a lower energy requirement [7, 51]. Therefore, this lower energy level may be attributed to the increased electron density resulting from the addition of electrophilic oxygen to the sulfur compounds [52].

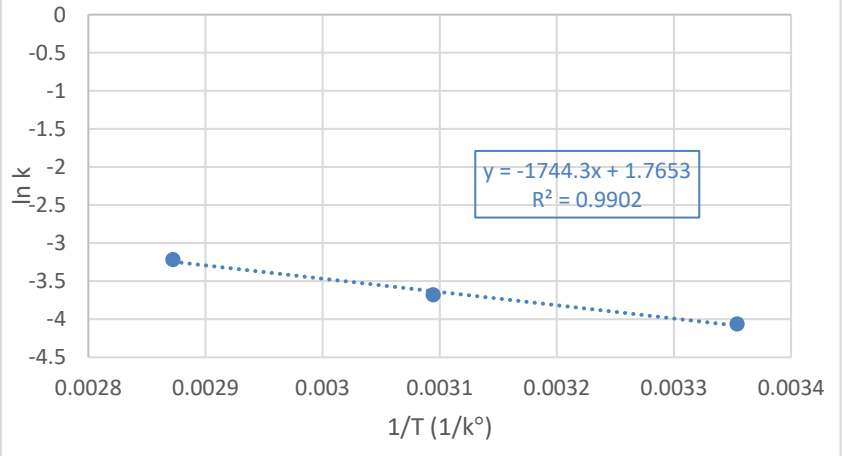


**Fig. 15.** ln (K١) versus (1/T) of ODS reactions using the prepared nano-catalyst

3.4. Comparison with previous studies

This research paper refers to a study of the ODS technique, comparing it with other studies that use silica as a catalyst support, based on desulfurization efficiency as shown in Table 4. The catalyst ($Fe_2O_3$ + NiO) / $SiO_2$ proved effective in achieving a good desulfurization rate of diesel fuel using ultrasonics.

**Table 4.** Comparison with previous studies

| Fuel | Type of catalyst | Type of reactor | Efficiency | Reference |
|---|---|---|---|---|
| Diesel | $MoO_3/SiO_2$ | batch reactor | 82% | [19] |
| Diesel | $H_{11}P_2W_{13}V_5O_{62}$/TMA-Si | batch reactor | 83% | [18] |
| Diesel | $C_{16}PW/SiO_2$ | batch reactor | 24.9% | [20] |
| Diesel | HPW/SiO2 | batch reactor | %٩8 | [17] |
| Diesel | 15%HPA–1/$SiO_2$ | batch reactor | 80% | [21] |

## 4- Conclusion

Oxidative desulfurization (ODS) is a promising alternative to conventional hydrodesulfurization (HDS) for producing ultra-low sulfur fuels under moderate operating conditions. In this study, a structured bimetallic catalyst ($Fe_2O_3$ + NiO)/$SiO_2$ was prepared using the incipient wetness impregnation method. The catalyst was characterized using XRD, BET, FTIR, TGA, and SEM-EDX techniques, with the results confirming the successful loading of iron and nickel oxides onto a silica substrate. BET analysis showed a decrease in surface area after metal loading from 166.47 to 149.57 m²/g, indicating an efficient distribution of active sites on the substrate surface. The prepared catalyst was then applied in an ultrasonic-assisted oxidative desulfurization process using real diesel fuel with a sulfur content of 2018.14 ppm. The effects of several variables, including temperature (25–75 °C), reaction time (30–60 mins), and ultrasonic efficiency (80–100%), were also investigated using hydrogen peroxide ($H_2O_2$) as the oxidizing agent.

The highest desulfurization efficiency of 90% was achieved under optimal conditions of 75 °C, 60 min reaction time, and 100% ultrasonic efficiency, followed by a 1:1 process using ethanol. The results also showed a significant improvement in the oxidative desulfurization reaction using ultrasound, as the ultrasonic probe enhanced dispersion and mixing by generating more bubbles, thus increasing the contact area and mass transfer between the liquid and solid phases. The reaction kinetics of the system were also studied and compared, showing adherence to a pseudo-first-order kinetic regime at the highest temperature.

The activation energy reached 14.50 kJ/mol, indicating the ease of oxidation of sulfur compounds under ultrasonic influence. These results confirm the efficiency of the prepared catalyst ($Fe_2O_3$–NiO/$SiO_2$) and the important role of ultrasound in enhancing the desulfurization process. The importance of reusing catalysts may lie in the need to demonstrate their activity and efficiency. However, the scope and objectives of this research focused specifically on generating a new catalyst, followed by the study of its reaction kinetics, pathway, and activation energy.

## Acknowledgement

This work is supported by the Department of Oil and Gas Refining/College of Petroleum Process Engineering/Tikrit University/ Iraq.

## Nomenclature

| Symbol | Description | Unit |
|---|---|---|
| API | American Petroleum Institute | …… |
| C | sulfur concentration | ppm |
| Ea | Activation energy | kJ/mole k |
| HDS | Hydrodesulfurizatio | …… |
| $H_2O_2$ | Hydrogen peroxide | ……. |
| $K_1$ | Rate constant for The pseudo-first order | 1/min |
| $K_2$ | Rate constant for pseudo- | 1/min.ppm |

| | | |
|---|---|---|
| | second-order | |
| $K_o$ | Frequency factor or pre-exponential factor | 1/sec |
| ODS | Oxidative desulfurization | …… |
| Pd | pore diameter | nm |
| Pv | pore volume | $cm^3/g$ |
| R | Universal gas constant | J / mole. K |
| T | Temperature of reaction | K |

## References


[1] M. N. Hossain, H. C. Park, and H. S. Choi, "A comprehensive review on catalytic oxidative desulfurization of liquid fuel oil," *Catalysts*, vol. 9, no. 3, p. 229, 2019, https://doi.org/10.3390/catal9030229

[2] C. Yang *et al.*, "Catalytic oxidative desulfurization of BT and DBT from n-octane using cyclohexanone peroxide and catalyst of molybdenum supported on 4A molecular sieve," *Separation and Purification Technology*, vol. 163, pp. 153–161, 2016, https://doi.org/10.1016/j.seppur.2016.02.050

[3] X. Tao *et al.*, "Inhibiting effects of nitrogen compounds on deep hydrodesulfurization of straight-run gas oil over a NiW/Al2O3 catalyst," *Fuel*, vol. 188, pp. 401–407, 2017, https://doi.org/10.1016/j.fuel.2016.09.055

[4] M. Riyadh and H. Alwan, "Sulfur Removal from Diesel Using Oxidative Desulfurization (ODS): A Case Study in MRC Refinery," *Journal of Energy Sustainability and Economics*, vol. 1, no. 1, pp. 1–7, 2025.

[5] G. Zhang, F. Yu, and R. Wang, "Research advances in oxidative desulfurization technologies for the production of low sulfur fuel oils," *Petroleum & Coal*, vol. 51, no. 3, pp. 196–207, 2009.

[6] F. F. Roman, J. L. Diaz de Tuesta, A. M. T. Silva, J. L. Faria, and H. T. Gomes, "Carbon-based materials for oxidative desulfurization and denitrogenation of fuels: A review," *Catalysts*, vol. 11, no. 10, p. 1239, 2021, https://doi.org/10.3390/catal11101239

[7] T. O. Sachdeva and K. K. Pant, "Deep desulfurization of diesel via peroxide oxidation using phosphotungstic acid as phase transfer catalyst," *Fuel processing technology*, vol. 91, no. 9, pp. 1133–1138, 2010, https://doi.org/10.1016/j.fuproc.2010.03.027

[8] G.-J. Wang, J.-K. Zhang, and Y. Liu, "Catalytic oxidative desulfurization of benzothiophene with hydrogen peroxide over Fe/AC in a biphasic model diesel-acetonitrile system," *Korean Journal of Chemical Engineering*, vol. 30, no. 8, pp. 1559–1565, 2013, https://doi.org/10.1007/s11814-013-0052-5

[9] H. Golchoubian and F. Hosseinpoor, "Effective oxidation of sulfides to sulfoxides with hydrogen peroxide under transition-metal-free conditions," *Molecules*, vol. 12, no. 3, pp. 304–311, 2007,https://doi.org/10.3390/12030304

[10] P. Huang, G. Luo, L. Kang, M. Zhu, and B. Dai, "Preparation, characterization and catalytic performance of HPW/aEVM catalyst on oxidative desulfurization," *RSC advances*, vol. 7, no. 8, pp. 4681–4687, 2017, https://doi.org/10.1039/C6RA26587A

[11] F. J. Cheburet, J. K. Kiptoo, and H. N. Wanyika, "Efficient release of urea with amorphous silica from pumice rock," *Scientific Reports*, vol. 15, no. 1, p. 35139, 2025, https://doi.org/10.1038/s41598-025-19142-z

[12] L. Gehrke, C. Bläker, C. Pasel, C. Farès, and D. Bathen, "Structural and energetic characterization of silica-alumina gels for adsorption processes," *Microporous and Mesoporous Materials*, vol. 365, p. 112891, 2024, https://doi.org/10.1016/j.micromeso.2023.112891

[13] A. Mekonnen *et al.*, "$Fe_2O_3$/NiO/C nanocomposite synthesis via the coprecipitation method for the photocatalytic degradation of methylene blue dye: synergetic effect," *Chemical Physics Impact*, p. 101005, 2026, https://doi.org/10.1016/j.chphi.2026.101005

[14] W. Ahmad *et al.*, "Oxidative desulfurization of petroleum distillate fractions using manganese dioxide supported on magnetic reduced graphene oxide as catalyst," *Nanomaterials*, vol. 11, no. 1, p. 203, 2021, https://doi.org/10.3390/nano11010203

[15] A. I. Zahran, E. M. El-Fawal, A. M. A. El Naggar, and T. F. Hassanein, "Production of low sulfur diesel fuel through ultrasonic catalytic oxidative route using novel mixed oxides nanocomposites assisted by solvent extraction," *Scientific Reports*, vol. 16, no. 1, p. 12058, 2026, https://doi.org/10.1038/s41598-026-39220-0

[16] K. A. T. Alviar, A. N. V Arbilo, S. S. Correa, and A. E. S. Choi, "Advanced desulfurization via ultrasonic-assisted oxidative methods in gasoline and crude oil towards sustainability," *Chemical Engineering Transactions*, vol. 114, pp. 55–60, 2024, https://doi.org/10.3303/CET24114010

[17] X. Yan, J. Lei, D. Liu, Y. Wu, and L. Guo, "Oxidative desulfurization of diesel oil using mesoporous phosphotungstic Acid/SiO2 as catalyst," *Journal of the Chinese Chemical Society*, vol. 54, no. 4, pp. 911–916, 2007, https://doi.org/10.1002/jccs.200700131

[18] F. Banisharif, M. R. Dehghani, M. del C. Capel-Sanchez, and J. M. Campos-Martin, "Highly catalytic oxidative desulfurization and denitrogenation of diesel using anchored-silica-gel vanadium-substituted Dawson-type polyoxometalate," *Catalysis Today*, vol. 333, pp. 219–225, 2019. https://doi.org/10.1016/j.cattod.2018.07.009

[19] R. Sundararaman and C. Song, "Catalytic oxidative desulfurization of diesel fuels using air in a two-step approach," *Industrial & Engineering Chemistry Research*, vol. 53, no. 5, pp. 1890–1899, 2014, https://doi.org/10.1021/ie403445f

[20] F. Liu *et al.*, "Facile Construction of Magnetic Ionic Liquid Supported Silica for Aerobic Oxidative Desulfurization in Fuel," *Catalysts*, vol. 11, no. 12, p. 1496, 2021, https://doi.org/10.3390/catal11121496

[21] R. Ghubayra, *Oxidative desulfurization of model diesel fuel catalyzed by polyoxometalates*. The University of Liverpool (United Kingdom), 2022.

[22] A. T. Albayrak and A. Tavman, "Sono-oxidative desulfurization of fuels using heterogeneous and homogeneous catalysts: A comprehensive review," *Ultrasonics Sonochemistry*, vol. 83, p. 105845, 2022, https://doi.org/10.1016/j.ultsonch.2021.105845

[23] L. Chmielarz, "Advances in selective oxidation of organic sulfides by hydrogen peroxide over titanium catalyst," *Chemistry and chemical technology*, 2025, https://doi.org/10.23939/chcht19.01.034

[24] D. Muktaly, Z. K. Myltykbaeva, Y. I. Imanbayev, A. K. Malayev, and A. Abylaikhan, "Experimental Investigation on Extraction of Oxidation Products of Sulfur-Containing Compounds," *Iranian Journal of Chemistry and Chemical Engineering*, vol. 45, no. 1, pp. 132–143, 2026, https://doi.org/10.30492/ijcce.2025.2057088.7063

[25] J. I. Humadi, A. A. Aabid, A. E. Mohammed, G. S. Ahmed, and M. A. Abdulqader, "New design of eco-friendly catalytic electro-photo desulfurization process for real diesel fuel," *Chemical Engineering Research and Design*, vol. 206, pp. 285–301, 2024, https://doi.org/10.1016/j.cherd.2024.05.001

[26] A. Karczmarska, W. Laskowska, D. Stróż, and K. Pawlik, "Inside the framework: structural exploration of mesoporous silicas MCM-41, SBA-15, and SBA-16," *Materials*, vol. 18, no. 15, p. 3597, 2025, https://doi.org/10.3390/ma18153597

[27] B. K. Al-Rawi and M. K. Ibrahem, "Synthesis and characterization of NiO nanoparticles prepared via plasma jet method," *Digest Journal of Nanomaterials & Biostructures (DJNB)*, vol. 20, no. 3, 2025, https://doi.org/10.15251/DJNB.2025.203.987

[28] M. M. Ilmi, N. Nurdini, E. Maryanti, P. Setiawan, and I. Ismunandar, "X-ray diffraction peak profile for determination of microstructural properties of hematite (Fe2O3)," *Journal of Research and Development on Nanotechnology*, vol. 1, no. 1, pp. 11–17, 2021.

[29] Y. L. Ni'mah, S. Suprapto, A. P. K. Subandi, N. E. Yuningsih, and A. C. Pertiwi, "The optimization of silica gel synthesis from chemical bottle waste using response surface methodology," *Arabian Journal of Chemistry*, vol. 15, no. 12, p. 104329, 2022, https://doi.org/10.1016/j.arabjc.2022.104329

[30] J. Bertaux, F. Froehlich, and P. Ildefonse, "Multicomponent analysis of FTIR spectra; quantification of amorphous and crystallized mineral phases in synthetic and natural sediments," *Journal of Sedimentary Research*, vol. 68, no. 3, pp. 440–447, 1998, https://doi.org/10.2110/jsr.68.440

[31] R. H. Ellerbrock, M. Stein, and J. Schaller, "Comparing silicon mineral species of different crystallinity using Fourier transform infrared spectroscopy," *Frontiers in Environmental Chemistry*, vol. 5, p. 1462678, 2024, https://doi.org/10.3389/fenvc.2024.1462678

[32] R. Ellerbrock, M. Stein, and J. Schaller, "Comparing amorphous silica, short-range-ordered silicates and silicic acid species by FTIR," *Scientific Reports*, vol. 12, no. 1, p. 11708, 2022, https://doi.org/10.1038/s41598-022-15882-4

[33] O. Hunfeld, R. H. Ellerbrock, M. Stein, C. W. Müller, and J. Schaller, "Analyzing the share of amorphous silica in mixtures with different soil minerals using fourier transform infrared spectroscopy and PLSR chemometrics," *Scientific Reports*, 2026, https://doi.org/10.21203/rs.3.rs-8192641/v1

[34] B. C. Smith, *Fundamentals of Fourier transform infrared spectroscopy*. CRC press, 2011.

[35] M. Rashwan, Z. Mao, J. S. Hirschi, T. J. Zuehlsdorff, M. Nyman, and A. Uysal, "Direct observation of carbon dioxide adsorption and binding at the air/aqueous interface," *PNAS nexus*, vol. 4, no. 3, p. pgaf064, 2025, https://doi.org/10.1093/pnasnexus/pgaf064

[36] S. Pasieczna-Patkowska, M. Cichy, and J. Flieger, "Application of Fourier transform infrared (FTIR) spectroscopy in characterization of green synthesized nanoparticles," *Molecules*, vol. 30, no. 3, p. 684, 2025, https://doi.org/10.3390/molecules30030684

[37] K. Al-Amin, M. Kawsar, M. T. R. B. Mamun, and M. S. Hossain, "Fourier transform infrared spectroscopic technique for analysis of inorganic materials: a review," *Nanoscale Advances*, vol. 7, no. 21, pp. 6677–6702, 2025, https://doi.org/10.1039/D5NA00522A

[38] J. H. Wall, "Spectroscopic Characterisation of Mesoporous Materials," 2011, *University of York*.

[39] C. M. R. Wright, K. Ruengkajorn, A. F. R. Kilpatrick, J.-C. Buffet, and D. O'Hare, "Controlling the surface hydroxyl concentration by thermal treatment of layered double hydroxides," *Inorganic chemistry*, vol. 56, no. 14, pp. 7842–7850, 2017, https://doi.org/10.1021/acs.inorgchem.7b00582

[40] A. T. Nawaf, A. T. Jarullah, and L. T. Abdulateef, "Design of a synthetic zinc oxide catalyst over nano-alumina for sulfur removal by air in a batch reactor," *Bulletin of Chemical Reaction Engineering & Catalysis*, vol. 14, no. 1, pp. 79–92, 2019, https://doi.org/10.9767/bcrec.14.1.2507.79-92

[41] A. T. Jarullah, B. A. Al-Tabbakh, M. A. Ahmed, S. A. Hameed, and I. M. Mujtaba, "Design of Novel Synthetic Iron Oxide Nano-Catalyst over Homemade Nano-Alumina for an Environmentally Friendly Fuel: Experiments and Modelling.," *Petroleum & Coal*, vol. 64, no. 4, 2022.

[42] J. I. Humadi, Y. S. Issa, D. Y. Aqar, M. A. Ahmed, H. H. Ali Alak, and I. M. Mujtaba, "Evaluation the performance of the tin (IV) oxide (SnO2) in the removal of sulfur compounds via oxidative-extractive desulfurization process for production an eco-friendly fuel," *International Journal of Chemical Reactor Engineering*, vol. 21, no. 6, pp. 727–741, 2023, https://doi.org/10.1515/ijcre-2022-0046

[43] A. T. Nawaf, A. T. Jarullah, S. A. Hameed, and I. M. Mujtaba, "Design of new activated carbon based adsorbents for improved desulfurization of heavy gas oil: experiments and kinetic modeling," *Chemical Product and Process Modeling*, vol. 16, no. 3, pp. 229–249, 2021. https://doi.org/10.1515/cppm-2020-0107

[44] J. I. Humadi, A. T. Nawaf, A. T. Jarullah, M. A. Ahmed, S. A. Hameed, and I. M. Mujtaba, "Design of new nano-catalysts and digital basket reactor for oxidative desulfurization of fuel: Experiments and modelling," *Chemical Engineering Research and Design*, vol. 190, pp. 634–650, 2023, https://doi.org/10.1016/j.cherd.2022.12.043

[45] R. J. Algawi, J. I. Humadi, and L. A. Khamees, "Experimental study of the impact of metal (iron, copper and aluminum) surface and light exposure on gum formation in Iraqi automotive gasoline," *Petroleum Science and Technology*, vol. 42, no. 21, pp. 2933–2944, 2024, https://doi.org/10.1080/10916466.2023.2179636

[46] G. H. A. Razzaq, K. I. Hamad, and J. I. Humadi, "Silver nanoparticles for ultrasonic assisted synthesis of oxidant agents in micro-reactor: kinetic analysis and process intensification," in *Materials science forum*, Trans Tech Publ, 2023, pp. 23–32. https://doi.org/10.4028/p-0brrx7

[47] Y. Yandy, N. F. Widyasari, T. Berliana, and M. Nasikin, "Heterogeneous Catalyst of Oxidative Desulfurization for Reducing Sulfur Content in Indonesia Biosolar," 2023, https://doi.org/10.5220/0011811800003575

[48] M. Rahimi, S. Shahhosseini, and S. Movahedirad, "Hydrodynamic and mass transfer investigation of oxidative desulfurization of a model fuel using an ultrasound horn reactor," *Ultrasonics sonochemistry*, vol. 52, pp. 77–87, 2019, https://doi.org/10.1016/j.ultsonch.2018.11.006

[49] B. M. Kumar, "Mechanistic Features of Ultrasound-Assisted Oxidative Desulfurization of Liquid Fuels," 2012, https://doi.org/10.1021/ie300807a

[50] J. I. Humadi, S. A. Gheni, S. M. R. Ahmed, and A. Harvey, "Dimensionless evaluation and kinetics of rapid and ultradeep desulfurization of diesel fuel in an oscillatory baffled reactor," *RSC advances*, vol. 12, no. 23, pp. 14385–14396, 2022, https://doi.org/10.1039/d2ra01663j

[51] W. Ahmad, I. Ahmad, and M. Yaseen, "Desulfurization of liquid fuels by air assisted peracid oxidation system in the presence of Fe-ZSM-5 catalyst," *Korean Journal of Chemical Engineering*, vol. 33, no. 9, pp. 2530–2537, 2016, https://doi.org/10.1007/s11814-016-0099-1

[52] Z. Hasan, J. Jeon, and S. H. Jhung, "Oxidative desulfurization of benzothiophene and thiophene with WOx/ZrO2 catalysts: effect of calcination temperature of catalysts," *Journal of hazardous materials*, vol. 205, pp. 216–221, 2012, https://doi.org/10.1016/j.jhazmat.2011.12.059

# دراسة تأثير المعلمات المختلفة على إزالة الكبريت بالأكسدة من وقود الديزل باستخدام المحفز ثنائي المعدن $Fe_2O_3$–$NiO/SiO_2$ : النماذج التجريبية والحركية

**محمد كمال صالح [١]، غسان حسن عبد الرزاق [١]، جاسم ابراهيم حمادي [١،*]**

*١ قسم هندسة تكرير النفط والغاز، كلية هندسة العمليات النفطية، جامعة تكريت، تكريت ٣٤٠٠١، العراق*

## الخلاصة

نظراً للمخاطر البيئية والصحية التي تُشكلها ملوثات الكبريت، يُعدّ التخلص منها وإنتاج وقود هيدروكربوني خالٍ من الكبريت أمراً بالغ الأهمية. ولذلك، أصبحت تقنية إزالة الكبريت التأكسدية (ODS) ضروريةً نظراً لكفاءتها العالية في ظل ظروف معتدلة. ركزت هذه الدراسة على تصنيع محفز $(Fe_2O_3 + NiO)/SiO_2$ باستخدام تقنية التشريب الرطب الأولي، متبوعةً بالتجفيف عند ١٢٠ درجة مئوية والتكليس عند ٦٠٠ درجة مئوية. أُجريت عدة اختبارات على المحفز قبل استخدامه، وهي: قياس مساحة السطح النوعية (BET)، والتحليل الحراري الوزني (TGA)، والتحليل الطيفي للأشعة السينية المشتتة للطاقة (SEM–EDX). أظهرت نتائج قياس مساحة السطح النوعية انخفاضاً في مساحة السطح من ١٦٦,٤٧ إلى ١٤٩,٥٧ $m^2/g$ بعد تحميل المعدن ، مما يؤكد تثبيت أكاسيد الحديد والنيكل على الدعامه السيليكا. أكدت تحليلات حيود الأشعة السينية (XRD) وتحليل طيف الأشعة تحت الحمراء بتحويل فوريه (FTIR) تكوّن طوري أكسيد المعدن $Fe_2O_3$ و NiO، مع الحفاظ على الطبيعة غير المتبلورة للسيليكا. تم اختبار المحفز المُحضر في عملية إزالة الكبريت التأكسدية بالموجات فوق الصوتية لوقود ديزل حقيقي يحتوي على ٢٠١٨,١٤ جزءًا في المليون من الكبريت، باستخدام بيروكسيد الهيدروجين كعامل مؤكسد. دُرست ظروف مختلفة، بما في ذلك تأثير درجة الحرارة (٢٥–٧٥ درجة مئوية)، وزمن التفاعل (٣٠–٦٠ دقيقة)، وشدة الموجات فوق الصوتية (٨٠–١٠٠%). تلا ذلك استخلاص بالإيثانول بنسبة ١:١ من الديزل إلى المذيب. وقد تحققت كفاءة إزالة للكبريت بلغت ٩٠%. أظهرت الدراسة أن التفاعل يتبع نموذجًا من الرتبة الأولى ، بثوابت سرعة تفاعل تبلغ ٠,٠١٧٢ و٠,٠٢٥٢ و٠,٠٤٠٠ $m^{-1}$ عند درجات حرارة ٢٥ و٥٠ و٧٥ درجة مئوية على التوالي، بمعاملات ارتباط تتجاوز ٠,٩٨. كما تم حساب طاقة التنشيط للتفاعل ووجد أنها تساوي ١٤,٥٠ كيلوجول/مول، مما يشير إلى ملاءمة الحركية وكفاءة النشاط التحفيزي تحت تأثير المعالجة بالموجات فوق الصوتية.

**الكلمات الدالة:** إزالة الكبريت التأكسدية (ODS)، وقود الديزل، دعامات السيليكا، المفاعل فوق الصوتي، المعلمات الحركية.